Chinese Chemical Letters 33 (2022) 2134–2138

Contents lists available at ScienceDirect

Chinese Chemical Letters

journal homepage: www.elsevier.com/locate/cclet

Sub-5 nm porous polymer decoration toward superhydrophobic MOFs with enhanced stability and processability

Siyi Rong, Pengcheng Su*, Shizheng Chen, Miaomiao Jia, Wanbin Li*

Guangdong Key Laboratory of Environmental Pollution and Health, School of Environment, Jinan University, Guangzhou 511443, China

ARTICLE INFO

Article history:
Received 9 July 2021
Revised 24 August 2021
Accepted 2 September 2021
Available online 8 September 2021

Keywords:
Metal-organic framework
Porous polymer decoration
Hydrophobicity
Stability
Processability

ABSTRACT

Metal-organic frameworks (MOFs) show great potential for various applications, but many of them suffer from the drawbacks of hydrolysis propensity and poor processability. Herein, we employ polymers of intrinsic microporosity (PIMs) with hydrophobic pores to decorate MOFs toward substantially improved water stability and shapeability. Through simple PIM-1 decoration, the sub-5 nm polymer layers can be uniformly deposited on MOF surfaces with almost no deterioration in porosity. Owing to the existence of superhydrophobic coating and the obstruction of water entrance into MOFs, the PIM-1 coated CuBTC exhibits impressive water resistance and excellent pore preservation ability after exposure in water, even in acidic and alkaline solutions. Moreover, polymer decoration improves the processability of MOFs, while various MOF/PIM-1 bulk wafers and oil-water separators can be obtained straightforwardly.

Metal-organic frameworks (MOFs), as a kind of porous crystalline materials coordinated with metal ions/clusters and organic linkers, show bright prospect and fabulous performance in numerous applications, such as, but not limited to, adsorption [1–4], molecular separation [5–7], catalysis [8–10], energy storage [11] and biomedicine [12], due to their exceptional porosities, large surface areas, and adjustable chemical properties. However, since metal-linker coordination bonds have propensity to be hydrolyzed, many of MOFs suffer from the bottleneck of poor moisture and water stability and may collapse in water and moist environments [13–15].

Various strategies have been developed for diminishing MOF vulnerability to water. Generally, design of MOFs with high-valent metal cations or hydrophobic linkers, *e.g.*, FMOF-1, UiO-66 and BIT-66, is beneficial to form forceful coordination bonds or build hydrophobic cavities for achieving admirable water resistance [16–20]. Unfortunately, for many MOFs with desirable function but poor stability, this fashion is unavailable. In order to ameliorate MOF stability to water, post-synthetic modification approaches, based on pore impregnation and surface decoration, are exploited for restraining the combination between water molecules and metal centers. For pore impregnation, the hydrophobic moieties are incorporated into the pores of frameworks and react with the active sites of MOFs [21–24]. Such as, the hydrophobic alkyl chains or aromatic acetylenes could be grafted or polymerized into MOFs to repel water association at metal centers for enhancing the moisture resistance [23,24]. Nevertheless, this method has strict requirements on the reactive sites of frameworks and inserted components, which will narrow the type scopes of MOFs to be modified and molecules used for grafting. Meanwhile, the inherent porosities and physicochemical characteristics will be degraded and altered. For surface decoration, the hydrophobic molecules or polymers are grafted or deposited on surface to prevent water from entering MOF inside [25–29]. For examples, MOF stabilization could be performed through grafting by fluorination michael addition and deposition of hydrophobic polydimethylsiloxane on crystal surfaces to restrict hydrolysis of coordination bonds [28,29]. Surface grafting is limited by the tedious procedures and the MOF reactive sites as well. Moreover, the additional nonporous layers may cause the declines in specific surface area and diffusion rate of molecules in coated layers. It is of greatly scientific interest to implement MOF stabilization in a facile and general manner under the premise of maintaining MOF properties.

Herein, we apply polymers of intrinsic microporosity (PIMs) with hydrophobic pores to decorate MOFs for simultaneously realizing MOF stabilization and pore preservation. Through simply immersion coating, an ultrathin polymer layer below 5 nm can be deposited on MOF surface for reducing the entry of water into MOFs (Fig. 1). The PIM-1 coated CuBTC shows the features of superhydrophobicity, well-maintained inherent pore accessibility, and substantially improved water stability, which can retain their crystalline structures and adsorption behaviors even after treating by acidic and alkaline aqueous solutions. Moreover, limited by the

* Corresponding authors.
E-mail addresses: pengchengsu@jnu.edu.cn (P. Su), gandeylin@126.com (W. Li).

https://doi.org/10.1016/j.cclet.2021.09.012
1001-8417/

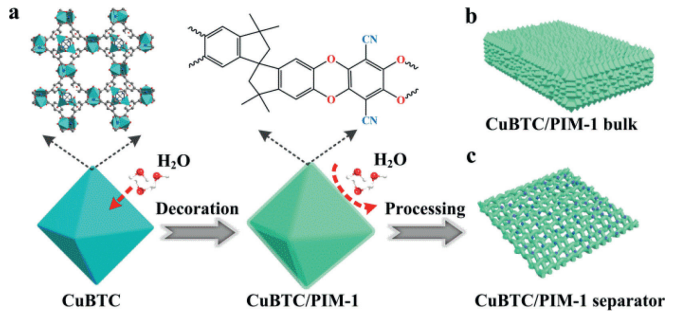

Fig. 1. PIM-1 decoration of MOFs. (a) Schematic illustration of PIM-1 decoration for improving water stability of MOFs. After decoration, the blue CuBTC turns to aquamarine of CuBTC/PIM-1. (b) Structure of the MOF/PIM-1 bulk wafer. (c) Structure of the MOF/PIM-1 separator.

features of insolubility and fragility, MOFs are far less processable than some other materials, for example polymers. The inferior processability is another drawback of MOFs for application. Profiting from the outstanding moldability of polymers, the PIM-1 decoration can make up the poorly processable issue of MOF crystals. Various MOF/PIM-1 bulk devices, including wafers and oil-water separators, can be straightforwardly prepared.

CuBTC, composed by paddle wheel copper centers and 1,3,5-benzenetricarboxylic acid (BTC) linkers, is promising for diverse applications but relatively sensitive to water [30,31]. PIM-1, consisted of rigid and contorted polymer chains, possesses superhydrophobic porous structures [32,33]. Thus, CuBTC and PIM-1 were employed as probes to demonstrate the feasibility of the reported simple coating method for improving water stability of MOFs. The PIM-1 powder, synthesized by polycondensation between 2,3,5,6-tetrafluoroterephthalonitrile and 5,5′,6,6′-tetrahydroxy-3,3,3′,3′-tetramethyl-1,1′-spirobisindane, exhibited Brunauer-Emmett-Teller (BET) specific surface area of 807 m^2/g and pore volume of 0.62 mL/g (Fig. S1 in Supporting information). For fabrication of CuBTC/PIM-1, the PIM-1 powder was dissolved in chloroform and then coated on the surface of CuBTC crystals by simple immersion method. The color of CuBTC/PIM-1 was aquamarine caused by the mixture of blue from CuBTC and yellow from PIM-1 (Fig. S2 in Supporting information). As observed from Fourier transform infrared (FTIR) spectrum of PIM-1 (Fig. 2a), there were characteristic peaks for –CH at 2955 cm^{-1}, –CN at 2240 cm^{-1} and C–O–C at 1265 and 1310 cm^{-1} [34]. The CuBTC and CuBTC/PIM-1 particles had analogous FTIR spectra with Cu-O peak at 730 cm^{-1} and O–C=O peak at 1365, 1455 and 1645 cm^{-1}. No obvious PIM-1 characteristic peaks in CuBTC/PIM-1 might be explained by too low PIM-1 content. X-ray photoelectron spectrophotometry (XPS) spectra illuminated the appearance of a new C–O–C peak and the increase of nitrogen content to 2.6%, which corroborated the successful PIM-1 decoration (Fig. 2b, Fig. S3 and Table S1 in Supporting information). It was noteworthy that the copper signal of CuBTC could still be observed in XPS spectrum of CuBTC/PIM-1, though the element content decreased from 5.3% to 1.8%. Considering the detection depth of XPS at several nanometers [35–37], it could be deduced that the PIM-1 coating layer was ultrathin.

Scanning electron microscopy (SEM) and optical microscopy images verified that the CuBTC and CuBTC/PIM-1 powders had similar octahedral structures (Fig. S4 in Supporting information). To visually examine the PIM-1 layer, transmission electron microscopy (TEM) images of CuBTC and CuBTC/PIM-1 were captured. It was clear that an ultrathin polymer layer below 5 nm was uniformly deposited on the CuBTC crystal (Fig. 2c and Fig. S5 in Supporting information), which agreed with the XPS and FTIR results. This decorated layer was much thinner than the deposited coats of MOF composites reported in previous studies with thickness of tens of nanometers at least [28,29]. X-ray energy dispersion spectroscopy mapping images of CuBTC/PIM-1 confirmed the homogeneous distributions of oxygen (CuBTC, PIM-1), carbon (CuBTC, PIM-1), copper (CuBTC) and nitrogen (PIM-1) (Fig. 2d). X-ray diffraction (XRD) patterns and nitrogen adsorption-desorption isotherms at 77 K were collected to study the crystalline and porous structures (Figs. 2e and f). For PIM-1, the bread peak in XRD pattern validated its amorphous structure. The CuBTC/PIM-1 displayed a consistent XRD pattern as experimental and simulated ones, suggesting the typical CuBTC textures and the intact crystalline structures after PIM-1 decoration (Fig. 2e). Nitrogen isotherms indicated that the BET specific surface area and pore volume of the CuBTC crystal were 1116 m^2/g and 0.61 mL/g, respectively. Given that the PIM-1 layer was ultrathin and porous, the CuBTC/PIM-1 exhibited almost the same porosity with surface area and pore volume of 1070 m^2/g and 0.60 mL/g, respectively (Fig. 2f and Table S2 in Supporting information). To study the thermal stability of CuBTC/PIM-1, thermogravimetric analysis (TGA) measurement was conducted in N_2 atmosphere. In Fig. S6 (Supporting information), the weight loss (8.5 wt%) of CuBTC/PIM-1 below 150 °C corresponded to the evaporation of water and guest molecules [38,39]. And a plateau could be captured within temperature range from 150 °C to 300 °C, indicating the good thermal stability of CuBTC/PIM-1 below 300 °C.

To investigate the stability, the prepared MOF powders were dispersed in water. After exposure for three days, by reason of hydrolysis, the deep blue CuBTC crystals changed to light blue (Fig. 3a). The morphology of H_2O-CuBTC became distorted from regular octahedron to rod and the XRD patterns varied dramatically (Figs. 3a and b, Fig. S7 in Supporting information), revealing its structural transformation. As well, the emergence of new -OH peak from $Cu(OH)_2$ at 3000-3300 cm^{-1} and the diversifications of Cu-O at 730 cm^{-1} and -COOH at 1720 cm^{-1} in FTIR spectrum of H_2O-CuBTC manifested the hydrolysis of coordination bonds and decomposition of chemical structures (Fig. S8 in Supporting information) [40]. As expected, the BET specific surface area and pore volume sharply dropped to 89 m^2/g and 0.11 mL/g, respectively (Fig. 2f and Table S2). All above results illustrated the serious corrosion of CuBTC caused by water molecule attack after water treatment. In contrast, the H_2O-CuBTC/PIM-1 showed hardly any changes in color, morphology, XRD pattern and FTIR spectrum compared with the original one (Figs. 3a and b, Figs. S7 and S8 in Supporting information). The porous merit of H_2O-CuBTC/PIM-1 was well-inherited, with BET specific surface area of 998 m^2/g and pore volume of 0.67 mL/g (Fig. 2f and Table S2). The identically crystalline, chemical, and porous properties of CuBTC/PIM-1 and H_2O-CuBTC/PIM-1 demonstrated that the MOF water stability had been substantially improved after PIM-1 decoration. As presented in Fig. 3c, the PIM-1 decoration had competitive porosity preservation capability during MOF modification and water treatment processes. The preservation ratios of surface areas after PIM-1 modification (P_M) and water treatment (P_W) for CuBTC/PIM-1 and H_2O-CuBTC/PIM-1 were calculated up to 96% and 93%, respectively (Table S3). These values were in good correlation with the above characterization results (*e.g.*, SEM, FTIR and XRD) and superior to those of most reported MOFs.

For understanding stabilization mechanism, we measured the water contact angles and water vapor adsorption-desorption behaviors of CuBTC and CuBTC/PIM-1. The water droplet was quickly absorbed by the CuBTC powder within 3 s, and the corresponding water contact angle was ~0° (Fig. 3d), suggesting the good hydrophilicity. Comparatively, for CuBTC/PIM-1, the spherical water droplet could be held on the powder, and the water contact angle reached as high as 155° (Fig. 3d). This phenomenon proved that the PIM-1 decoration endowed the CuBTC/PIM-1 composite with superhydrophobicity. Fig. 3e showed the water vapor isotherms

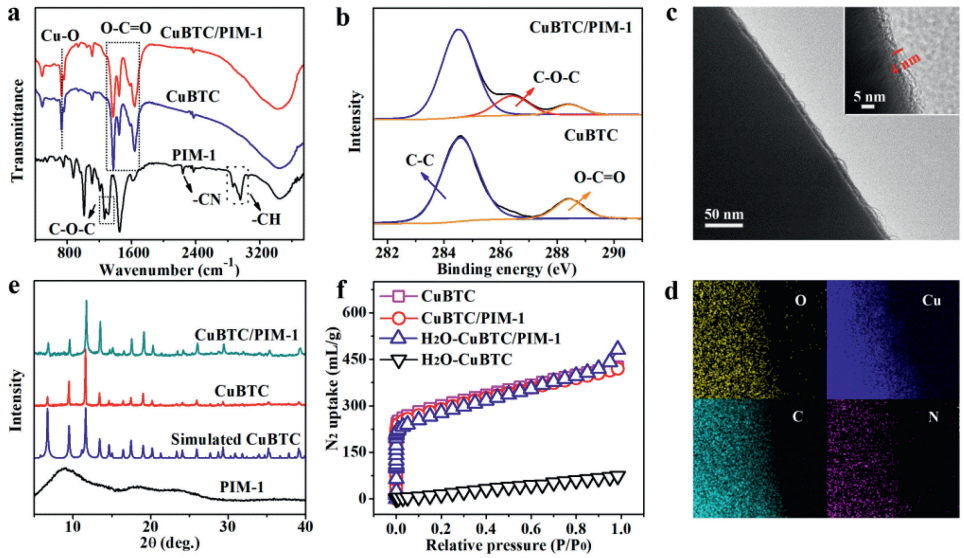

Fig. 2. Characterizations of CuBTC/PIM-1. (a) FTIR spectra of PIM-1, CuBTC and CuBTC/PIM-1. (b) C 1s XPS spectra of CuBTC and CuBTC/PIM-1. (c) TEM images of CuBTC/PIM-1. (d) X-ray energy dispersion spectroscopy mapping images of CuBTC/PIM-1. (e) XRD patterns of PIM-1, simulated CuBTC, CuBTC and CuBTC/PIM-1. (f) Nitrogen uptakes of CuBTC, CuBTC/PIM-1, H_2O-CuBTC and H_2O-CuBTC/PIM-1 at 77 K.

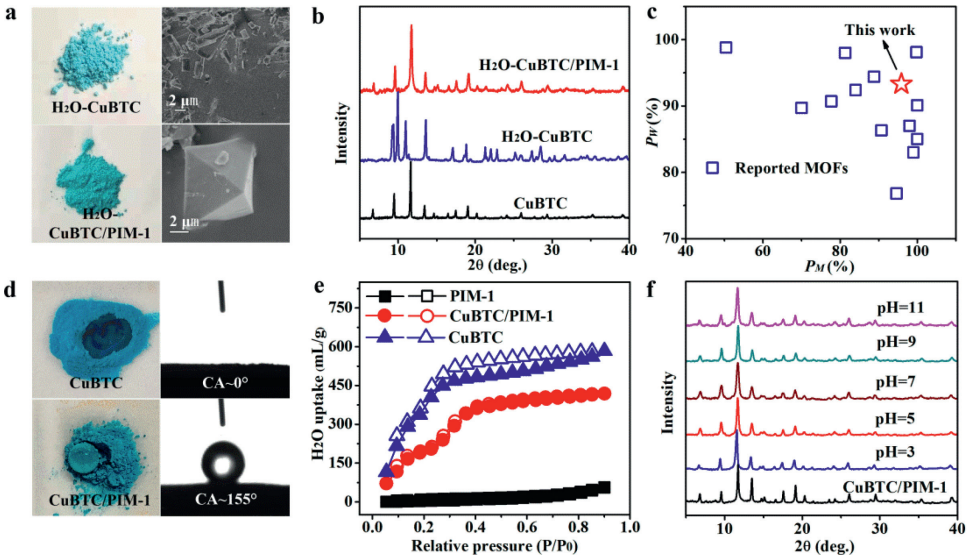

Fig. 3. Stability of CuBTC/PIM-1. (a) Digital photographs and SEM images of H_2O-CuBTC and H_2O-CuBTC/PIM-1 after water treatment for three days. (b) XRD patterns of H_2O-CuBTC and H_2O-CuBTC/PIM-1 after water treatment for three days. XRD pattern of CuBTC is presented for comparison. (c) Comparison of MOF/PIM-1 in this study with other modified MOFs for preservation ratios of BET specific surface areas. P_M and P_W are preservation ratios during modification and water treatment processes, respectively. The related data are listed in Table S3 (Supporting information). (d) Digital photographs and water contact angle images of CuBTC and CuBTC/PIM-1. (e) Water vapor adsorption-desorption isotherms of PIM-1, CuBTC, and CuBTC/PIM-1 at 298 K. (f) XRD patterns of CuBTC/PIM-1 after treating by acidic and alkaline solutions with different pH for three days.

of PIM-1, CuBTC, and CuBTC/PIM-1. The PIM-1 powder had typical water vapor adsorption-desorption curves of porous materials with superhydrophobic pores [41]. As a result of open metal sites, the CuBTC particle possessed good hydrophilicity with rapid adsorption at low pressure and high water uptake of 582 mL/g. Meanwhile, owning to the strong affinity of metal centers to water molecules, a clear hysteresis loop appeared in isotherms [41]. For CuBTC/PIM-1, the water adsorption capacity had great reduction to 416 mL/g, especially at low pressure. Interestingly, the adsorption for CuBTC/PIM-1 took longer times to reach equilibrium than that for CuBTC, indicating the effective limitation of water molecule diffusion through PIM-1 layers. Therefore, the significantly improved water resistance of CuBTC/PIM-1 was attributed to the remarkably enhanced hydrophobicity and the effective hindrance of PIM-1 to water. We further assessed the stability of MOF/PIM-1 under harsh conditions, through exposure in acidic and alkaline solutions with different pH for three days. The unaltered XRD patterns testified that CuBTC/PIM-1 maintained its intrinsic crystalline structures (Fig. 3f). The identical characteristic peaks of FTIR spectra for CuBTC/PIM-1 after treatment in different acidic and alkaline solutions revealed the unvaried chemical structures (Fig. S9 in Supporting information). These results confirmed the commendable stability of the CuBTC/PIM-1 even under harsh conditions.

Gas adsorption properties of the prepared MOF materials before and after water treatment were evaluated at 298 K. All MOFs showed gas adsorption capacities with order of CO_2 and N_2 (Figs. 4a and b), which were in accordance with the quadrupole moments and polarizabilities of three gases [42,43]. Thanks to

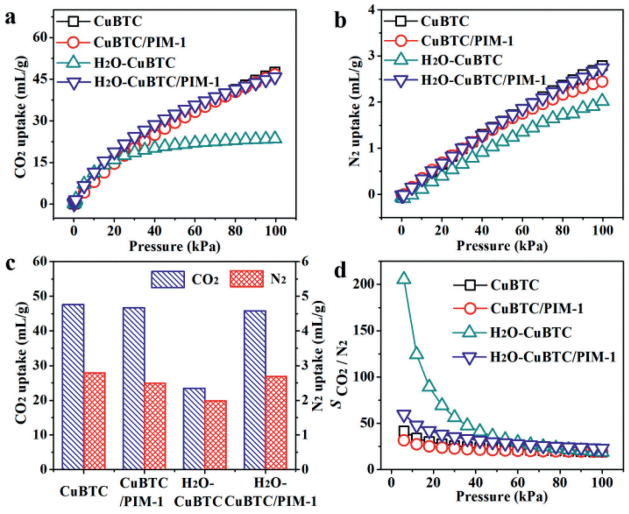

Fig. 4. Gas adsorption performances. (a) CO_2 and (b) N_2 adsorption isotherms of CuBTC, CuBTC/PIM-1, H_2O-CuBTC, and H_2O-CuBTC/PIM-1. (c) CO_2 and N_2 uptakes of CuBTC, CuBTC/PIM-1, H_2O-CuBTC, and H_2O-CuBTC/PIM-1. (d) CO_2/N_2 adsorption selectivity. The selectivity was calculated by ideal adsorption solution theory based on fitting adsorption isotherms with single-site Langmuir-Freundlich model. The H_2O-CuBTC and H_2O-CuBTC/PIM-1 samples were prepared by treating CuBTC and CuBTC/PIM-1 in water for three days, respectively.

the well-maintained pore accessibility from ultrathin porous layer and the unprecedented stability of the MOF composite, the CuBTC/PIM-1 and H_2O-CuBTC/PIM-1 powders displayed similar gas uptakes as CuBTC, with CO_2 adsorption capacities in the range of 45–48 mL/g at 100 kPa, respectively (Fig. 4c and Table S4 in Supporting infomation). It should be noted, the difference in times of equilibrium adsorption for three materials was negligible, which illustrated that the ultrathin and porous PIM-1 layers did not affect the gas diffusion in MOFs. Conversely, the gas uptakes of H_2O-CuBTC deteriorated grievously, yet the CO_2 adsorption capacities were still achieved at 23.5 mL/g, respectively. Compared with the decline ratios of surface area (92%) and pore volume (82%), the reduction of CO_2 (51%) adsorption capacity was not so severe. The CO_2 adsorption isotherm of H_2O-CuBTC was more convex than other prepared MOFs, with larger growth rate at low pressure related to maximum adsorption capacity (Fig. S10 in Supporting infomation). Gas adsorption behavior is governed by porous features and active sites of adsorbents. The serious deformation in surface area and pore volume of H_2O-CuBTC resulted in the degeneration of gas uptakes, while the existence of Cu(II) metal sites and the exposure of polar carboxyl groups in decomposed CuBTC after hydrolysis still contributed to gas adsorption [40,44]. Hence, the H_2O-CuBTC particle had less degradation of gas adsorption than porosity and showed more convex isotherms than other MOFs. The CO_2/N_2 adsorption selectivity was calculated by ideal adsorption solution theory based on fitting adsorption isotherms with single-site Langmuir-Freundlich model. For CO_2/N_2 (50:50) system, the CuBTC CuBTC/PIM-1, H_2O-CuBTC and H_2O-CuBTC/PIM-1 powders showed similar selectivity about 20 at 100 kPa (Fig. 4d and Table S4). Because of the more convex curve for CO_2, the H_2O-CuBTC powder had higher CO_2/N_2 selectivity at low pressure than others. Relative to water-vulnerable CuBTC, the superhydrophobic and water-stable CuBTC/PIM-1 displayed invariable gas adsorption capacity and selectivity, even after water treatment.

For crystalline MOF materials, the inferior processability is one of bottlenecks for application [45–48]. Inspired by the excellent moldability of polymers, we attempted to shape MOFs into bulk materials by combining PIM-1. Through solidification of the CuBTC/PIM-1 suspension in a cylindrical mold, the CuBTC/PIM-1 bulk wafer with high MOF content of 97 wt% could be prepared simply (Fig. 5a). The PIM-1 polymer could play the role of glue to bond the CuBTC particles together. Besides molding bulk materials, the MOF/PIM-1 could be coated on the surfaces of various materials. We decorated the polypropylene (PP) textile fiber nets from masks by MOF/PIM-1. After deposition of CuBTC/PIM-1, the white fiber net changed to aquamarine (Fig. 5b). The prepared CuBTC/PIM-1/PP net had remarkable hydrophobicity but excellent

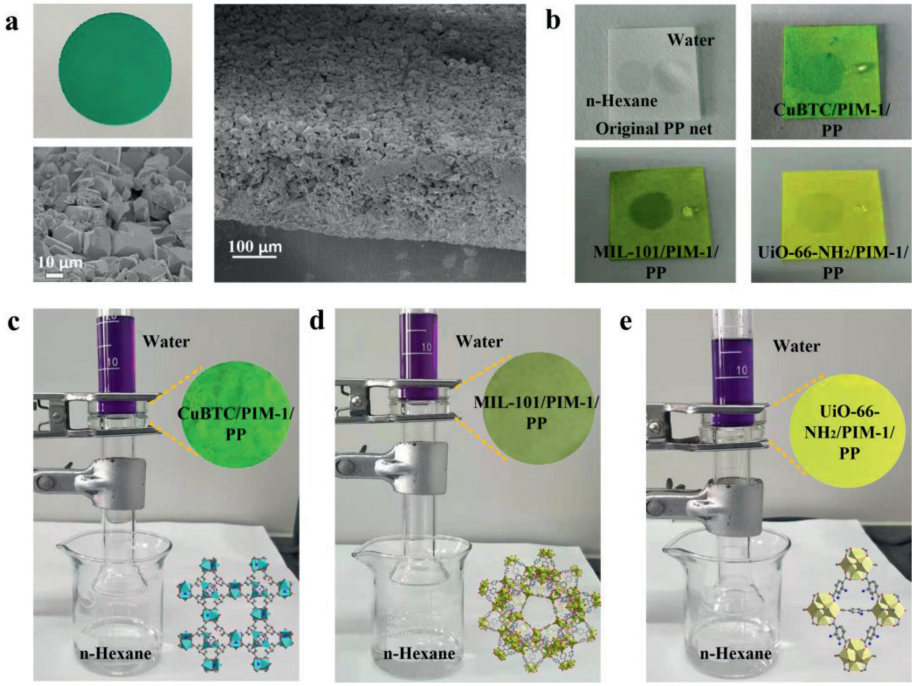

Fig. 5. Applicability of PIM-1 decoration. (a) Digital photograph and SEM images of CuBTC/PIM-1 bulk wafer. (b) Digital photographs of the original PP net, CuBTC/PIM-1/PP, MIL-101/PIM-1/PP and UiO-66-NH_2/PIM-1/PP nets. The water and *n*-hexane droplets were dropped on nets for illuminating the hydrophobicity and lipophilicity, respectively. (c-e) Digital photographs of the CuBTC/PIM-1/PP, MIL-101/PIM-1/PP, and UiO-66-NH_2/PIM-1/PP nets for oil-water separation. The water was colored by dye for clarifying.

n-hexane wettability. Intrigued by these merits, the CuBTC/PIM-1/PP net was applied for separating oil-water mixture. As shown in Fig. 5c, the transparent organic *n*-hexane phase immediately and totally passed through the CuBTC/PIM-1/PP separator and entered into the beaker, while the purple water was intercepted completely with the separation efficiency large than 99%. The reproducibility test of CuBTC/PIM-1/PP in the oil-water separation was conducted. As shown in Fig. S11 (Supporting information), the separation efficiency of CuBTC/PIM-1/PP was not influenced by the cycle time and maintained above 99%, proving its excellent recyclability. The XRD patterns of CuBTC/PIM-1/PP before and after oil-water separation were measured and displayed in Fig. S12 (Supporting information). Obviously, the CuBTC/PIM-1/PP displayed good stability and maintained its crystal structure after five cycles of oil-water separation. To present the universality of decoration, the MIL-101, composed by chromium-based centers and 1,4-benzenedicarboxylic acid linkers, and UiO-66-NH_2, made by zirconium-based centers and 2-aminoterephthalic acid linkers, were further utilized for coating on the PP nets. The green MIL-101/PIM-1/PP and yellow UiO-66-NH_2/PIM-1/PP separators exhibited fantastic hydrophobicity and lipophilicity (Fig. 5b), and displayed excellent oil-water separation performances with the separation efficiencies all above 99% (Figs. 5d and e).

In summary, we developed a facile, mild, and versatile strategy for improving the water resistance of MOFs, based on the combination of porous polymers with hydrophobic pores. The PIM-1 layers with ultrathin thickness below 5 nm were uniformly coated on MOF surfaces by simple immersion. Because of the ultrathin and porous properties of the polymer layers, the PIM-1 coated CuBTC showed almost no decrease in surface area and pore volume. Since the PIM-1 layers could endow CuBTC/PIM-1 with superhydrophobicity and provide the hindrance for water into MOFs, the prepared composites had substantially enhanced stability to water and could keep their crystalline and chemical structures, porous features, and gas adsorption performances after exposure in water for several days at least, even in acidic and alkaline solutions. Moreover, the introduction of polymers facilitated the processability of MOFs. Through simple polymer solidification, the MOF/PIM-1 could be shaped into bulk wafer using molds and coated on nets to prepare oil-water separators. Overall, the strategy reported herein offers an alternative route for obtaining MOF composites and devices with impressive stability and performance in a scalable, highly processable and general manner.

Declaration of competing interest

The authors report no declaration of interest.

Acknowledgments

This work was financially supported by National Natural Science Foundation of China (No. 51708252) and Guangdong Basic and Applied Basic Research Foundation (Nos. 2020B1515120036, 2021A1515010187).

Supplementary materials

Supplementary material associated with this article can be found, in the online version, at doi:10.1016/j.cclet.2021.09.012.

References

[1] H. Furukawa, K.E. Cordova, M.O' Keeffe, O.M. Yaghi, Science 341 (2013) 1230444.
[2] Y. Qi, J. Liu, W. Zheng, et al., Chin. Chem. Lett. 29 (2018) 959–962.
[3] O. Alduhaish, B. Li, H. Arman, et al., Chin. Chem. Lett. 28 (2017) 1653–1658.
[4] W. Wu, J. Su, M. Jia, et al., Sci. Adv. 6 (2020) eaax7270.
[5] Y. Peng, Y. Li, Y. Ban, et al., Science 346 (2014) 1356–1359.
[6] W. Li, P. Su, Z. Li, et al., Nat. Commun. 8 (2017) 406.
[7] Y. Xia, C. Wang, M. Yu, X. Bu, Chin. Chem. Lett. 32 (2021) 1153–1156.
[8] M. Zhao, K. Yuan, Y. Wang, et al., Nature 539 (2016) 76–80.
[9] D. Ma, B. Li, Z. Shi, Chin. Chem. Lett. 29 (2018) 827–830.
[10] S. Goswami, H. Noh, L.R. Redfern, et al., Chem. Mater. 31 (2019) 1485–1490.
[11] Y. Gu, L. Miao, Y. Yin, et al., Chin. Chem. Lett. 32 (2021) 1491–1496.
[12] M. Taheri, D. Ashok, T. Sen, et al., Chem. Eng. J. 413 (2021) 127511.
[13] J. Li, Y. Wang, Y. Yu, Q. Li, Chin. Chem. Lett. 29 (2018) 837–841.
[14] L.N. McHugh, M.J. McPherson, L.J. McCormick, et al., Nat. Chem. 10 (2018) 1096–1102.
[15] K. Jayaramulu, F. Geyer, A. Schneemann, et al., Adv. Mater. 31 (2019) 1900820.
[16] N. Nijem, P. Canepa, U. Kaipa, et al., J. Am. Chem. Soc. 135 (2013) 12615–12626.
[17] H. Furukawa, F. Gándara, Y.-B. Zhang, et al., J. Am. Chem. Soc. 136 (2014) 4369–4381.
[18] S. Yuan, L. Feng, K. Wang, et al., Adv. Mater. 30 (2018) 1704303.
[19] D. Ma, P. Li, X. Duan, et al., Angew. Chem. Int. Ed. 59 (2020) 3905–3909.
[20] M.W. Logan, J.D. Adamson, D. Le, F.J. Uribe-Romo, ACS Appl. Mater. Interfaces 9 (2017) 44529–44533.
[21] D. Sun, P.R. Adiyala, S.J. Yim, D.P. Kim, Angew. Chem. Int. Ed. 58 (2019) 7405–7409.
[22] J.X. Wang, Y. Muhammad, Z. Gao, et al., Chem. Eng. J. 404 (2021) 126562.
[23] J.G. Nguyen, S.M. Cohen, J. Am. Chem. Soc. 132 (2010) 4560–4561.
[24] N. Ding, H. Li, X. Feng, et al., J. Am. Chem. Soc. 138 (2016) 10100–10103.
[25] Q. Sun, H. He, W.Y. Gao, et al., Nat. Commun. 7 (2016) 13300.
[26] X.M. Zheng, S. Liu, S. Rehman, et al., Chem. Eng. J. 289 (2020) 123424.
[27] X. Qian, F. Sun, J. Sun, et al., Nanoscale 9 (2017) 2003–2008.
[28] Y. Wu, Z. Lv, X. Zhou, et al., Chem. Eng. J. 355 (2019) 815–821.
[29] W. Zhang, Y. Hu, J. Ge, et al., J. Am. Chem. Soc. 136 (2014) 16978–16981.
[30] S.S.Y. Chui, S.M.F. Lo, J.P.H. Charmant, et al., Science 283 (1999) 1148–1150.
[31] M. Rivera-Torrente, L.D.B. Mandemaker, M. Filez, et al., Chem. Soc. Rev. 49 (2020) 6694–6732.
[32] M. Carta, R. Malpass-Evans, M. Croad, et al., Science 339 (2013) 303–307.
[33] F. Feizi, M. Shamsipur, M.B. Gholivand, et al., J. Mater. Chem. C 8 (2020) 13827–13835.
[34] M. Yahia, Q.N. Phan Le, N. Ismail, et al., Microporous Mesoporous Mater. 312 (2021) 110761.
[35] H. Li, Z. Song, X. Zhang, et al., Science 342 (2013) 95–98.
[36] J. Rubio-Zuazo, P. Ferrer, G.R. Castro, J. Electron. Spectrosc. Relat. Phenom. 180 (2010) 27–33.
[37] J. Yan, A.D. Carl, A.R. Maag, et al., Dalton Trans. 48 (2019) 4520–4529.
[38] F. Xu, Y. Yu, J. Yan, et al., Chem. Eng. J. 303 (2016) 231–237.
[39] S. Loera-Serna, J. Flores, A.M. Navarrete-Lopez, et al., Chem. Eur. J. 25 (2019) 4398–4411.
[40] G. Majano, O. Martin, M. Hammes, et al., Adv. Funct. Mater. 24 (2014) 3855–3865.
[41] J. Canivet, A. Fateeva, Y. Guo, et al., Chem. Soc. Rev. 43 (2014) 5594–5617.
[42] P. Chowdhury, C. Bikkina, S. Gumma, J. Phys. Chem. C 113 (2009) 6616–6621.
[43] H. Huang, H. Sato, T. Aida, J. Am. Chem. Soc. 139 (2017) 8784–8787.
[44] D. Peralta, G. Chaplais, A. Simon-Masseron, et al., J. Am. Chem. Soc. 134 (2012) 8115–8126.
[45] Y. Chen, X. Huang, S. Zhang, et al., J. Am. Chem. Soc. 138 (2016) 10810–10813.
[46] V.J. Pastore, T.R. Cook, J. Rzayev, Chem. Mater. 30 (2018) 8639–8649.
[47] W. Li, Prog. Mater. Sci. 100 (2019) 21–63.
[48] G.W. Peterson, K. Au, T.M. Tovar, H. T, Chem. Mater. 31 (2019) 8459–8465.